

Critical Role of Membrane Cholesterol in Exocytosis Revealed by Single Platelet Study

Shencheng Ge[†], James G. White[‡], and Christy L. Haynes^{†,*}

[†]Department of Chemistry, Institute of Technology and [‡]Department of Laboratory Medicine, Pathology and Pediatrics, School of Medicine, University of Minnesota, Minneapolis, Minnesota 55455

Exocytosis is a fundamental cellular process critical for a wide range of cellular functions (1). It is defined as the transport of chemical messenger-containing vesicles/granules to the plasma membrane and subsequent fusion and content release to the extracellular space (2–4). Numerous cell types, including neurons, endocrine cells, and platelets to name a few (1), use exocytosis to deliver chemical messengers for specific biological tasks. Given the critical function of exocytosis, a number of key protein components of the exocytotic machinery, such as the SNARE (soluble *N*-ethylmaleimide-sensitive factor attachment protein receptor) protein family, have been identified and characterized (5–8); however, the critical role of membrane lipids has not been fully appreciated. Membrane lipid species not only constitute the platform for exocytosis but also actively regulate exocytosis. Cholesterol is an important lipid species in this regard (9). Despite its long-recognized abundance, influence on overall biochemical and biophysical lipid properties, and ubiquity in the mammalian lipid membrane, the role of cholesterol in exocytosis has not been fully defined.

The current mechanistic understanding of cholesterol in regulating exocytosis has been largely derived from studies on several commonly employed secretory cell models, including chromaffin cells and its closely related immortal cell line PC12 cells (9–13). While the use of these secretory cell models has generated invaluable insight about exocytosis, they are nonideal partially because the manipulation of cholesterol content in the cell and/or granule membrane often leads to unpredictable downstream effects, given its versatile role in modulating cellular functions. The resultant downstream effects may significantly complicate data interpretation and thus impede thorough mechanistic understanding. For instance, alterations of quantal size (*i.e.*,

ABSTRACT Exocytosis is a fundamental cellular process, pivotal in a wide range of cell types, used to deliver chemical messengers from one cell to another cell or tissue. While a tremendous amount of knowledge has been gained in the past several decades about the exocytotic machinery, recently it has become clear that the role of membrane lipids is also crucial in this process. In particular, the critical role of the abundant and ubiquitous cholesterol molecules has not been well-defined. Early insight has been gleaned from single cell amperometric studies on several commonly used secretory cell models, including chromaffin cells and PC12 cells; however, these secretory cell models are not ideal because manipulations of membrane cholesterol content may influence downstream cholesterol-dependent processes, making data interpretation difficult. Herein, blood platelets are employed as a simpler secretory cell model based on their anuclear nature and unique chemical messenger exocytosis behavior. Carbon-fiber microelectrochemistry was employed to measure real-time exocytosis from single platelets with depleted or enriched cholesterol either in the naturally occurring form or as the synthetic analogue epicholesterol. The experimental results show that membrane cholesterol directly modulates the secretion efficiency of individual platelets, as well as the kinetics of secretion events. Moreover, substitution of platelet membrane cholesterol with epicholesterol yields exocytotic behavior indistinguishable from that of normal platelets, arguing against the possibility of cholesterol-specific interactions in regulating exocytosis. It is clear from this work that membrane cholesterol plays a critical biophysical, rather than biochemical, role in platelet exocytosis and likely in exocytosis in general.

*Corresponding author,
chaynes@umn.edu.

Received for review May 11, 2010
and accepted June 30, 2010.

Published online June 30, 2010

10.1021/cb100130b

© 2010 American Chemical Society

granule content of a given stored chemical messenger) induced by the manipulation of membrane cholesterol content make accurate interpretation of the measured secretion kinetics difficult (10, 11, 14). In fact, not only does membrane cholesterol influence granule content, but other endogenous (15) and exogenous (16) lipid species in these secretory cell models do as well. An ideal cell model for fundamental studies of lipid characteristic effects on exocytosis would have granules that are minimally influenced by changes in cholesterol or other lipid species.

Platelets, a populous secretory cell in the bloodstream that serves a myriad of functions, use the evolutionarily conserved SNARE machinery to drive exocytosis (17) and possess several highly desirable cellular features that make them uniquely suited for reliable and selective examination of membrane cholesterol during exocytosis. One fortuitous platelet exocytotic feature is that secretable molecules are differentially sorted to separate classes of secretory granules in a molecular size-dependent manner. Dense-body granules (DG) selectively store small molecules and ions, such as serotonin and Ca^{2+} , whereas α -granules contain larger molecules, such as proteins (18). This unusual feature eliminates hurdles encountered when using other secretory cell models (e.g., PC12 cells) to study cholesterol and exocytosis by decoupling the interplay between the granule membrane and the granule content during exocytosis (19, 20). This interplay is unfavorable because the observed proteinaceous granule matrix swelling (e.g., in chromaffin cells (19, 20)) following initial membrane fusion may act as the main driving force to promote further membrane fusion; this makes the selective examination of the membrane-derived driving forces and thus the cholesterol influence on exocytosis difficult. This difficulty is exacerbated when carbon-fiber microelectrochemistry techniques, the gold standard for monitoring real-time exocytosis (14), are employed because these techniques measure exocytosis based on the outward flux of stored electroactive molecules (e.g., catecholamine from chromaffin cells). This flux becomes insensitive to the membrane dynamics during exocytosis when the rate-limiting factor controlling molecule flux is the effective chemical messenger diffusivity in the swelling granule matrix rather than the membrane unfolding process (as is clearly the case in mast cells (21)). Platelets, however, do not have these difficulties. First, the membrane cholesterol content is naturally decou-

pled from the quantal size (i.e., serotonin content) because platelets do not synthesize serotonin but rather take it up dynamically from the bloodstream. Once taken up, these molecules are stably sequestered in DGs. Second, the interplay between the granule membrane and the granule content is likely negligible because platelets uniquely sequester small molecules as an aggregate devoid of expandable matrix, making the carbon-fiber microelectrochemistry measurements capable of revealing the membrane dynamics during exocytosis based on the measurement of released electroactive molecules (i.e., serotonin from platelets (22, 23)). While the patch-clamp method is an alternative approach to acquire similar data, it would require exquisite control to study the exceedingly small platelets. Another fortuitous property of platelets is that they do not rapidly recycle granules, likely due to their physiological role, making the lipid dynamics of the cell membrane during exocytosis much less complicated for platelets than for those cells that rapidly recycle granules (e.g., chromaffin cells (24)).

Several additional platelet features facilitate their use as the secretory cell model herein. First, platelets are readily accessible in high purity and quantity, a clear advantage over tissue-derived secretory cells. Second, platelets are small. Discoid platelets are 2–3 μm in diameter and approximately 1 μm in thickness; thus, the platelet volume ($\sim 3\text{--}7\text{ fL}$) is only a fraction of a typical 10- μm -diameter mammalian cell ($\sim 523\text{ fL}$ for a chromaffin cell), indicating that platelets can harbor significantly fewer secretory granules (e.g., less than 10 DGs per human platelet (25) vs $\sim 10,000$ vesicles per rat chromaffin cell (26)). This feature makes the often used exclusion criteria for overlapping amperometric spikes unnecessary and thus eliminates possible bias. Lastly, platelets do not have nuclei; therefore, these cells retain only minimal capability for *de novo* protein synthesis (27). In fact, platelets inherit the majority of their organelles and molecules from their precursor megakaryocytes (27), suggesting that platelets are simple and stable cells well-suited for cholesterol and exocytosis study.

This study exploits the combination of carbon-fiber microelectrochemistry and a novel lipid substitution approach to clearly define some, if not all, aspects of the role of cholesterol in exocytosis for platelets and perhaps secretory cells in general. First, the efficient cholesterol-complexing reagent, methyl- β -cyclodextrin

(M β CD), is used to manipulate the cholesterol level in platelets (28), and the exocytotic behavior is examined in real time using carbon-fiber microelectrochemistry. In addition, epicholesterol, a synthetic analogue of cholesterol, is substituted for the naturally occurring cholesterol to investigate the specificity of cholesterol's role in exocytosis (29).

RESULTS AND DISCUSSION

Effects of Altered Membrane Cholesterol on Dense-Body Granule Secretion. Although the subcellular distribution of cholesterol in platelets is not pursued in this study, a large majority of the free cholesterol is likely to be present in the plasma membrane (30), and thus the total cholesterol level is used as a cholesterol index for the plasma membrane cholesterol content. Incubation with 10 mM M β CD for 30 min removed approximately 32% of the cholesterol content present in the control condition. Enrichment of cholesterol in cholesterol-depleted platelets and control platelets with cholesterol-saturated M β CD yielded cholesterol content slightly higher than the normal level ($111.2 \pm 2.3\%$ vs control, $p < 0.01$) for the cholesterol-depleted platelets and significantly higher than the control ($131.8 \pm 2.7\%$ vs control, $p < 0.001$) for undepleted platelets. Ultrastructural analysis by TEM revealed that platelets under all four conditions maintained regular DGs (Figure 1, panels a–d and insets). Morphological alterations of the overall platelet diameter and thus volume, as well as the open canalicular system, a three-dimensional lipid membrane structure present in platelets, are discernible; however, unlike the spherical shape of the dense bodies, these features are difficult to quantify solely on the basis of TEM analysis. Despite the minor observed ultrastructural changes, all platelets were able to spread similarly on the poly-L-lysine-coated coverslips that were used for electrochemical measurements, indicating that platelets maintained viability under conditions investigated herein (Supplementary Figure S1). With this capability to modulate the plasma membrane cholesterol levels with minimal cell disruption in a preferred cell model, we are uniquely positioned to investigate how cholesterol influences exocytotic behavior. Variations in cholesterol levels may influence either chemical behavior (e.g., the ability to localize SNARE proteins) or physical properties of the membrane (e.g., fluidity, rigidity) or both. Real-time measurements of platelet exocytosis will reveal whether the chemical/physical char-

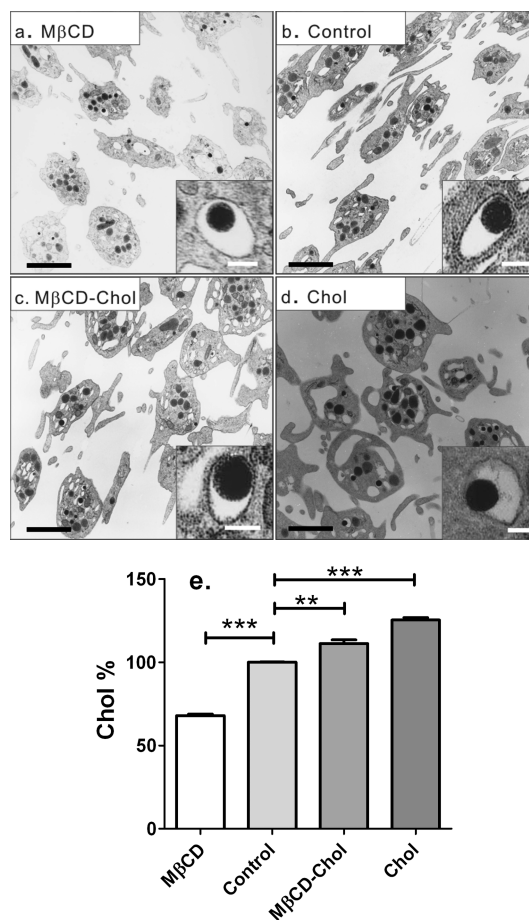


Figure 1. Ultrastructural analysis of platelet morphology and cholesterol quantification. The four conditions examined are (a) cholesterol depletion, (b) control, (c) cholesterol depletion followed by cholesterol enrichment, and (d) cholesterol enrichment alone. Scale bar: 1 μ m with inset scale bar, 100 nm. The total cholesterol content (e) was determined using a cholesterol oxidase assay and normalized to the control condition. Data are expressed as mean \pm standard deviation. $N = 3$ for each condition, $**p < 0.01$, $***p < 0.001$, using a two-tailed unpaired Student's t test.

acteristics of a cholesterol-rich membrane enhances fusion pore formation, maintenance, and dilation. In addition, this model system, in combination with a sterol substitution scheme, presents the unique opportunity to separate biochemical and biophysical effects of cholesterol during exocytosis.

Following manipulation of cholesterol content, real-time measurements of DG secretion from single plate-

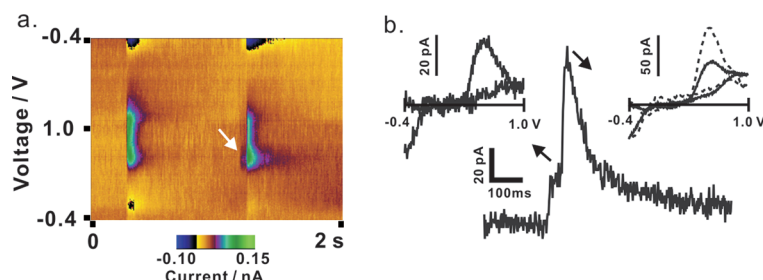


Figure 2. Exocytotic event recorded by fast-scan cyclic voltammetry. The false-color plot (a) was constructed on the basis of the oxidation and reduction current (encoded by color) recorded at the carbon-fiber microelectrode when its potential was rapidly ramped from -0.4 to 1.0 V and back to -0.4 at 2000 V s^{-1} every 2 ms . Each vertical 2 ms “slice” and the full 2D representation are a single scan and a stack of consecutive single scans, respectively. The second event at $\sim 1.3\text{ s}$ displays a small current (white arrow, termed foot feature) prior to the major current feature. The reconstructed amperometric response using the oxidation peak current value (at $\sim 0.6\text{ V}$) obtained on each consecutive scan and the cyclic voltammograms using two single scans obtained from the foot feature and the major current spike are plotted in panel b. The cyclic voltammograms (solid line, insets in panel b) show identical oxidation ($\sim 0.6\text{ V}$)/reduction ($\sim -0.4\text{ V}$, partially shown) peak locations and peak separation compared to those obtained from a standard serotonin solution (dotted line) and thus confirm the secreted molecules as serotonin during both the foot and full fusion events.

lets were performed using carbon-fiber microelectrochemistry. Herein, this method was first exploited to probe the properties of the fusion pore, which is often short-lived and only maintained for a measurable period of time in a minority of fusion events (22, 31). While it is commonly accepted that granule content leakage *via* fusion pore causes the appearance of a small current signal, known as a “foot” (31), immediately preceding the major spike on an amperometric trace (e.g., Figure 3, panel c), there has been no direct dynamic evidence to support this phenomenon in platelets. The false-color plot (Figure 2, panel a) obtained using fast-scan cyclic voltammetry at the carbon-fiber microelectrode confirms that this is indeed the case. The color plot shows one secretion event with no apparent fusion pore leakage (a full fusion event) and a second secretion event with a sustained fusion pore ahead of the full fusion event. The reconstructed amperometric response (at $+600\text{ mV vs Ag/AgCl}$) for the second fusion event clearly shows a small current signal (*i.e.*, a “foot” feature) ahead of the full fusion spike, corresponding to maintenance of a nanometric fusion pore for tens of milliseconds prior to dilation and exocytosis of the majority of serotonin. Cyclic voltammograms obtained from the foot and full fusion spike (Figure 2, panel b) are identical to

that measured using a standard serotonin solution. The oxidation/reduction peak locations and peak separation on the cyclic voltammogram represent an electrochemical signature for a given electroactive species; the close superposition of these characteristics (Figure 2, panel b) obtained from single platelet measurements and a standard serotonin solution positively confirms that serotonin secretion to the extracellular space is responsible for both amperometric current features (*i.e.*, foot and major spike).

Once the molecular identity has been confirmed by fast-scan cyclic voltammetry, constant-potential amperometry at the carbon-fiber microelectrode was utilized to measure real-time exocytosis from single platelets because of its superior time resolution (22, 23). A typical amperometric trace collected from a single rabbit platelet (Figure 3, panel a) has ~ 20 spikes, corresponding to ~ 20 DGs. Due to the small number of secretion events, nearly all of the spikes are well-separated and baseline-resolved within the amperometric traces; therefore, spike exclusion criteria are not necessary due to minimal spike overlap. To examine the overall effect of cholesterol on platelet secretion behavior, the cumulative percentage of all secretion events collected from the same condition is first plotted and compared (Figure 3, panel b). The plots show that the majority of the DGs are secreted within the first 30 s following activation by ionomycin, an ionophore capable of raising intracellular Ca^{2+} levels. The overall rate of secretion, characterized by the rising slope, is slower for platelets treated with M β CD (*i.e.*, the cholesterol-depleted platelets) compared to the other three conditions (which are similar). Clearly, the enrichment of cholesterol in M β CD-treated platelets successfully restores the overall secretion efficiency, indicating that the observed change is specific to cholesterol rather than unintended side-effects of M β CD treatments. The cholesterol-dependent overall exocytotic efficiency is likely influenced by the ability of membrane cholesterol to organize exocytotic machinery in the plasma membrane, as cholesterol is known to spatially coordinate essential SNARE proteins within cholesterol-enriched microdomains at fusion sites (12, 32–34). Upon cholesterol depletion from platelets, cholesterol-enriched microdomains are likely disrupted, leading to the dispersion of the platelet SNARE proteins (35) from such microdomains. Consequently, the otherwise efficient exocytotic machinery is compro-

mised, as indicated by the retarded overall secretion rate measured herein.

Detailed analysis of the individual spike characteristics yields rich information about the kinetics of granule content release, which in turn reflects the membrane unfolding process during platelet exocytosis. Four major parameters are examined herein, including Q , the quantal size or the amount of serotonin secreted from each DG, and three kinetic parameters, T_{rise} , $T_{1/2}$, and T_{decay} (Figure 3, panel c, and see Methods for definition). As expected, quantal size remains the same for all conditions with altered cholesterol content due to the decoupling between the membrane cholesterol content and the granule content. However, the overall trend for all three kinetic parameters is that increased cholesterol content correlates with longer secretion time. For example, $T_{1/2}$, the time widely used to characterize the discharge of granular content, decreases from the control condition value of 9.3 ± 1.0 ms (mean \pm SEM) to 5.8 ± 0.6 ms for the cholesterol depletion condition, accelerating secretion by nearly a factor of 2. Among the kinetic parameters, T_{rise} , the time characterizing the fusion pore dilation rate, is most sensitive to the membrane cholesterol content. This parameter correlates remarkably well with the total cholesterol content in platelets with a correlation coefficient of $R^2 = 0.98$. Not only does cholesterol have a critical effect on the parameters characterizing the delivery rate of chemical messengers from platelet granules, cholesterol also influences the ability of the platelet to maintain the fusion pore structure, manifested as the “foot” feature on the amperometric trace. In the control condition, approximately $17.4 \pm 2.7\%$ of the spikes displayed a foot feature. This foot occurrence decreases to $9.0 \pm 1.6\%$ and increases to $29.1 \pm 3.3\%$ for cholesterol depletion and cholesterol enrichment conditions, respectively. Again, the re-delivery of cholesterol to cholesterol-depleted platelets restored the foot occurrence to the control cell level (Figure 3, panel h). Interestingly, the enrichment of cholesterol in the untreated platelets significantly augmented the foot occurrence. Further quantitative analysis of the foot features revealed a good correlation between the total cholesterol content and three parameters considered herein, $I_{\text{foot}}/I_{\text{spike}}$ ($R^2 = 0.82$, Figure 3, panel i), $T_{\text{foot}}/T_{1/2}$ ($R^2 = 0.68$, Figure 3, panel j), and $Q_{\text{foot}}/Q_{\text{spike}}$ ($R^2 = 0.76$, Figure 3, panel k). From these quantitative analyses, it is clear that membrane cholesterol profoundly affects the ability of platelets to discharge

the granular content by influencing multiple steps in the exocytotic process, including fusion pore formation, dilation, and full fusion.

Effects of Epicholesterol Substitution on Dense-Body Granule Secretion. To further explore the nature of the observed cholesterol-dependent secretion behavior, the naturally occurring cholesterol molecules in platelets were substituted by the synthetic analogue epicholesterol. This substitution experiment is done to examine the possibility of exocytotic regulation *via* cholesterol-specific interactions with components critical in exocytosis, such as SNARE proteins. Cholesterol and epicholesterol differ structurally only in the spatial orientation of the hydroxyl group at the 3β chiral center (Figure 4, panel a). This subtle structural difference, however, leads to a drastic difference in their respective oxidation efficiency by cholesterol oxidase; cholesterol oxidase efficiently oxidizes only cholesterol but not its stereoisomer epicholesterol (Supplementary Figure S2). In addition, this structural difference also leads to significantly different orientation of these two molecules in the lipid membrane and thus likely their specific interactions with membrane-embedded proteins (29, 36); however, the differences in the physical properties of cholesterol- and epicholesterol-enriched lipid membrane are rather minimal (37, 38). Therefore, the use of epicholesterol may facilitate the discrimination between biochemical and biophysical roles of cholesterol in various lipid membrane-based processes. For exocytosis, this approach offers a unique opportunity to test the hypothesis that cholesterol-specific interactions are critical in regulating exocytosis, which has remained virtually unexplored thus far (9).

To test this hypothesis in a well-controlled manner, three conditions were optimized so that depleted cholesterol was replaced by an equal amount of epicholesterol (Figure 4, panel b, and Supplementary Figure S3). Extent of cholesterol removal from platelets was controlled by varying M β CD concentration and incubation time. Epicholesterol was delivered to platelets *via* epicholesterol-saturated M β CD, and approximately 34% of cholesterol content in the untreated platelets was replaced with epicholesterol after 15 min incubation with 5 mM epicholesterol-saturated M β CD. Amperometry measurements on epicholesterol-loaded platelets revealed the kinetics for the overall cell and individual granule secretion behavior upon epicholesterol substitution. In line with the aforementioned de-

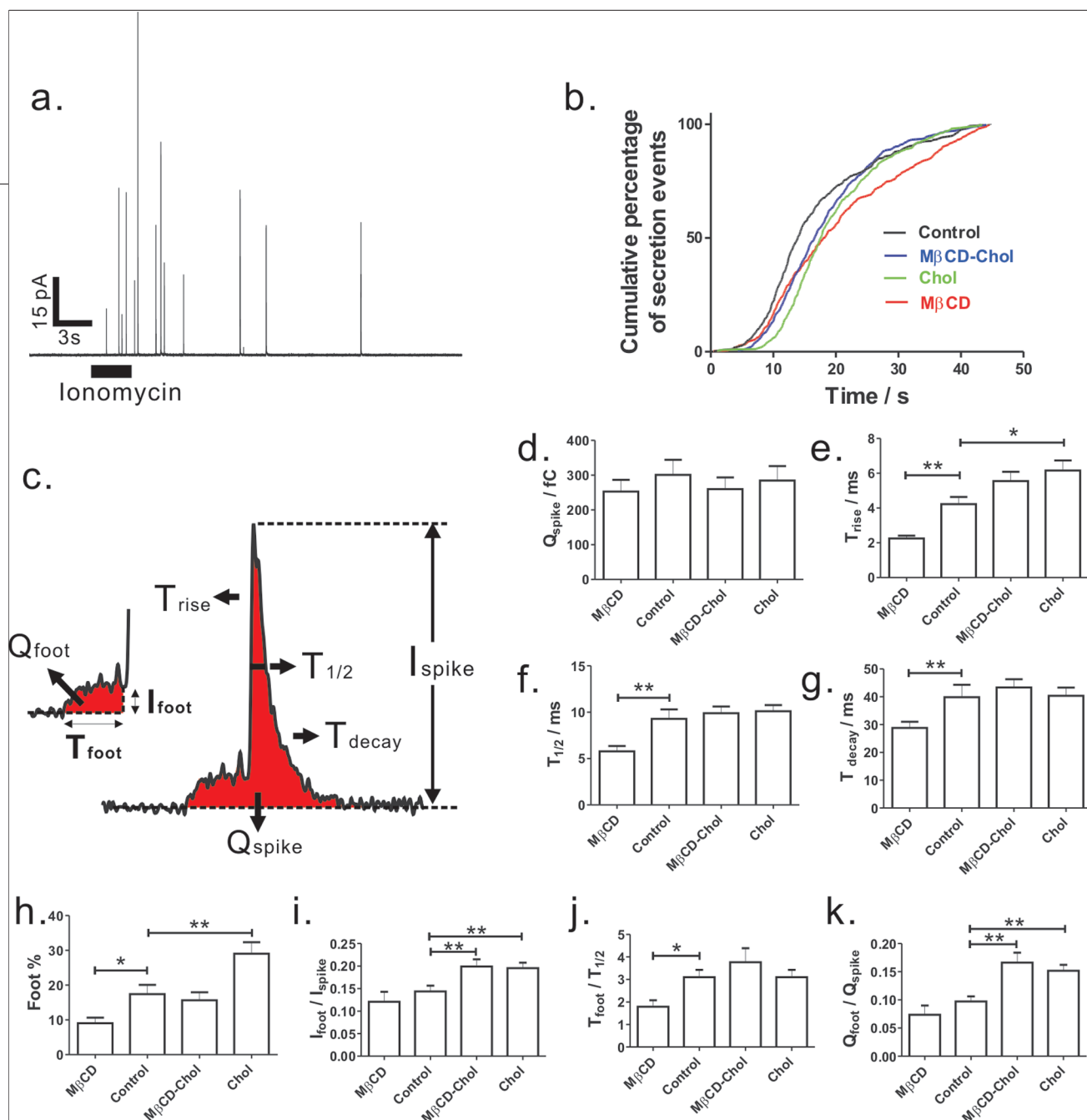


Figure 3. Amperometric measurements of dense-body granule secretion. **a)** A typical amperometric trace is shown with the black bar indicating the onset and duration of stimulant application. **b)** Cumulative percentage of secretion events are plotted using the individual spike time pooled together for a given condition. The total number of spikes for MβCD, MβCD-Chol, Control, and Chol are 428, 468, 519, and 494, respectively. **c)** Spike parameters used to characterize secretion are denoted (see Methods for definitions). **d–g).** Spike characteristics: Q , T_{rise} , $T_{1/2}$, and T_{decay} (mean \pm SEM) are plotted in the order of increasing cholesterol content from left to right. **h–k).** Foot occurrence and foot parameters: $I_{\text{foot}}/I_{\text{spike}}$, $T_{\text{foot}}/T_{1/2}$, and $Q_{\text{foot}}/Q_{\text{spike}}$ (mean \pm SEM) characterize the foot feature relative to the spike that immediately follows. $N = 25$ platelets for panels d–h. $N = 41, 95, 72$, and 155 foot features, for MβCD, Control, MβCD-Chol and Chol, respectively. * $p < 0.05$ and ** $p < 0.01$, using a two-tailed unpaired Student's t test.

crease in overall release efficiency upon cholesterol depletion (Figure 3, panel b), the condition with the lower cholesterol level displayed a slower overall secretion rate (Figure 4, panel c). The substitution with epicholesterol not only restored but slightly enhanced this rate. Analysis of the individual secretion events revealed a similar trend for T_{rise} and foot occurrence (Figure 4,

panels e and f). T_{rise} and foot occurrence decreased significantly when cholesterol content was further lowered from $76.1 \pm 1.3\%$ to $44.4 \pm 0.6\%$, consistent with the trends in Figure 3, panels e and h, respectively. The redelivery of epicholesterol restored the T_{rise} from 2.2 ± 0.1 ms to 2.5 ± 0.1 ms and foot occurrence from $5.0 \pm 0.7\%$ to $11.4 \pm 0.9\%$, respectively. Neither T_{rise} nor

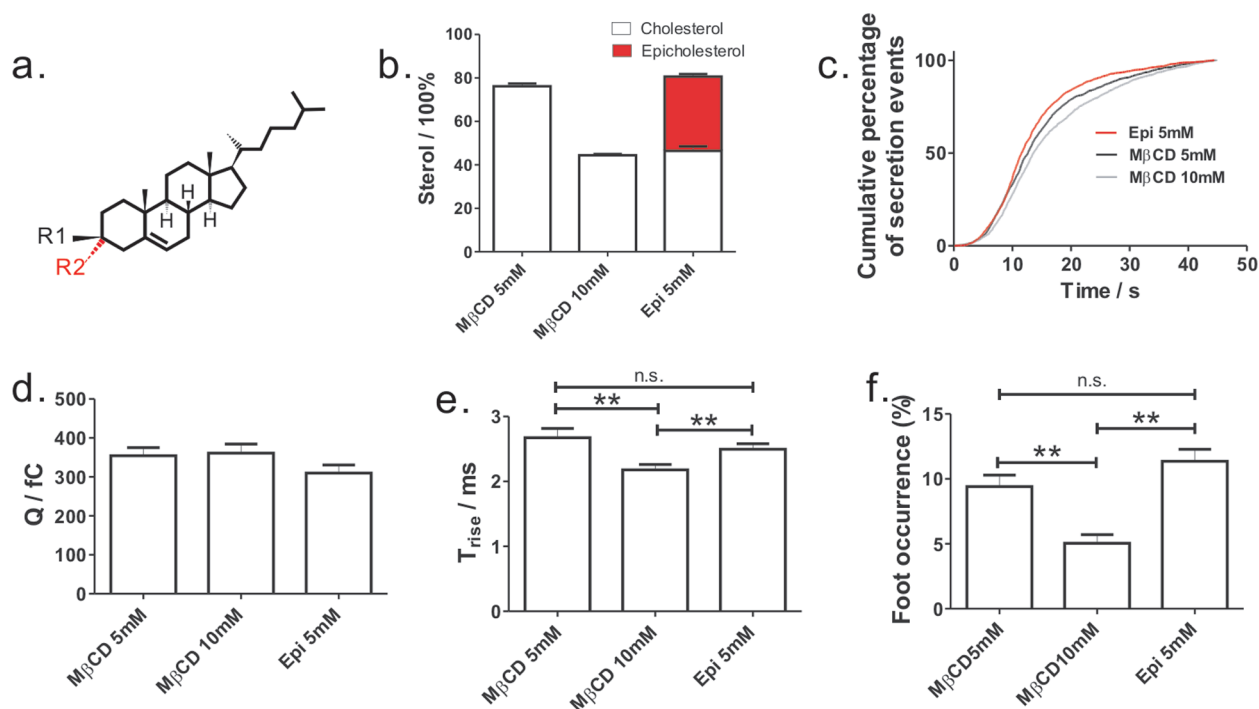


Figure 4. Epicholesterol substitution effect on dense-body granule secretion. **a)** Structures are shown for cholesterol (R1 = OH, R2 = H) and epicholesterol (R1 = H, R2 = OH). **b)** The total cholesterol and epicholesterol content quantified by GC-FID is expressed as a molar percentage with respect to the untreated control condition. Data are expressed as mean \pm SD and $N = 3$ for all conditions. **c)** The cumulative percentage of secretion events are plotted using the spikes pooled from 105 platelets collected from four separate experiments. The total number of spikes are 1593, 1626, and 2010 for MβCD 10 mM, MβCD 5 mM, and Epi 5 mM, respectively. **d–f)** Amperometric spike characteristics: Q , T_{rise} , foot occurrence (mean \pm SEM) are compared. $N = 105$ platelets, and $**p < 0.01$ using a two-tailed unpaired Student's t test. In panels **e** and **f**, no statistical difference (n.s.) is also denoted.

foot occurrence characteristics for the epicholesterol-reloaded condition are distinguishable from that for the high cholesterol condition (*i.e.*, MβCD 5 mM condition, $p > 0.05$). Again, no quantal size change was observed for any conditions (Figure 4, panel d). The substitution experiments provide evidence arguing against a biochemical role for cholesterol in exocytosis, though it is not definitive because of the coexistence of cholesterol and epicholesterol after substitution. In addition, it is possible that epicholesterol substitution has subtle effects on the SNARE proteins or other protein components that do not manifest in changes to the exocytotic process.

Biophysical Role of Cholesterol in Dense-Body Granule Secretion Based on a Stalk Model. Taken together, the experimental results strongly indicate that membrane cholesterol plays a critical biophysical role in platelet DG secretion. Perhaps the most critical physi-

cal characteristic of cholesterol in modulating platelet DG exocytosis is its negative curvature (9). In the classic stalk model of lipid membrane fusion (39, 40), the negatively curved cholesterol molecules (41) are thought to stabilize key intermediate structures along the membrane fusion pathway and therefore lower the energy required for membrane fusion to proceed. The early intermediate stalk structure has a highly negative curvature (Figure 5, panel d) as the outer granule leaflet initially merges with the inner cell membrane leaflet, and this curvature persists throughout the fusion process (Figure 5, panels d–f). Cholesterol may accumulate at these sites and stabilize the structure on the basis of its intrinsic negative curvature. Large positive curvature is also created at the late fusion-pore stage where the inner granule membrane leaflet eventually coalesces with the outer cell membrane leaflet; however, it is not readily evident if cholesterol will destabi-

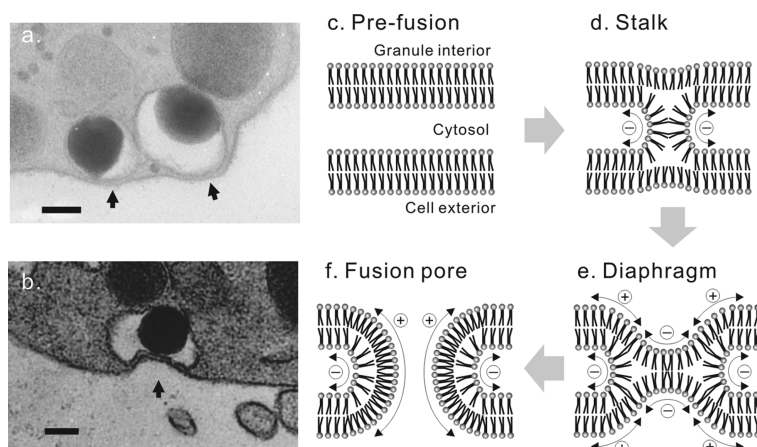


Figure 5. Stalk model for membrane fusion. Electron micrographs (a) and (b) depict the close juxtaposition of dense-body granules to the cell membrane and arrows point to possible fusion sites. In a rare case (b), the dense body granule appears to be deformed. Scale bars: 100 nm. On the basis of the stalk model, the membrane fusion must proceed through the key intermediates, including (d) stalk, (e) diaphragm, and (f) fusion pore, along the fusion pathway. Membrane leaflet curvatures for the key intermediates are labeled.

lize this positively curved leaflet because cholesterol may or may not be concentrated in this region of the membrane. Cholesterol could be either preferentially excluded from this region due to the conflicting curvature, based on passive diffusion from the site, or concentrated in this region if the fusion predominantly occurs within the cholesterol-enriched microdomains (12). It becomes more challenging to accurately evaluate the influence of cholesterol on fusion-pore properties if possible participating SNARE proteins are also included in this pure lipid-based stalk model, because the actual composition and structure of the fusion pore intermediate has not yet been clearly defined and is, in fact, the source of ongoing debate (42). Nevertheless, the stalk model supports that cholesterol stabilizes the leaflets facing the cytosol at the fusion site throughout the fusion process. This stabilizing effect likely increases the probability for platelets to maintain the fusion-pore intermediate and also decelerates the overall membrane unfolding process, which agrees with the observed higher foot occurrence (Figure 3, panel h) and longer granule secretion time for the high cholesterol conditions (Figure 3, panels e–g). Indeed, such possible contribution to exocytosis based on the negative curvature of cholesterol was supported by cholesterol substitution experiments using native cortical vesicles

from sea urchins. In this work by Churchward *et al.*, it was demonstrated that ensemble homotypic vesicle fusion was recovered by redelivery of lipid species with similar or larger intrinsic negative curvature compared to that of cholesterol (43). Besides the physical character of negative curvature, cholesterol may also exert its impact on membrane fusion on the basis of its long-recognized role in modulating the physical properties of the lipid membrane, such as viscosity and fluidity. During exocytosis, granule membrane and cell membrane lipid species must intermix (44), and alteration of cell membrane cholesterol content likely influences the in-membrane diffusivities of membrane constituents and thus changes the subsequent intermixing kinetics of the granule and cell membranes during exocytosis (*i.e.*, the membrane unfolding process). Both biophysical factors of cholesterol are likely critical in influencing the stability of the fusion-pore intermediate in platelets and also other secretory cell types including chromaffin cells (10) and PC12 cells (11), based on the observed similar cholesterol-dependent foot behaviors. Not only does membrane cholesterol have a profound impact on the foot behavior, it also modulates the secretion kinetics of the main spike in platelet exocytosis, reflecting the cholesterol-induced alterations of the membrane unfolding process following fusion-pore intermediate (Figure 3, panels e–g). The use of other secretory cell models such as chromaffin cells, however, failed to reveal such cholesterol dependency (10–12). As previously discussed, carbon-fiber microelectrochemistry measures the outward electroactive molecule flux through the dilating fusion pore. Unfortunately, it becomes insensitive to membrane unfolding processes at the late stages of exocytosis in most cell types when the outward flux is limited by the slow diffusion of molecules out of the swelling proteinaceous matrix rather than the membrane unfolding process. In contrast, the protein-matrix-free DGs allow the membrane unfolding dynamics throughout exocytosis to be studied and reveal previously inaccessible information about cholesterol's influence on exocytosis.

To summarize, the results presented herein clearly show that exocytotic behavior in platelets is dependent on cellular cholesterol content and strongly supports a biophysical role for cholesterol in regulating exocytosis. The use of this greatly simplified secretory cell model, platelets, favorably permits the membrane-derived driving forces for exocytosis to be selectively examined. This

work provides a previously inaccessible mechanistic understanding of cholesterol in platelet exocytosis and perhaps for exocytosis in general due to the evolution-

ary conservation of exocytotic machinery (3) and the ubiquitous nature of cholesterol in mammalian cells.

METHODS

For procedures on preparation of washed platelets, manipulation of cholesterol/epicholesterol content in platelets, cholesterol and epicholesterol quantification, and transmission electron microscopy analysis, see Supporting Information.

Carbon-Fiber Microelectrode Fabrication and Electrochemical Measurements. The procedure for carbon-fiber microelectrode fabrication followed a published protocol (23). All electrochemical measurements were performed on an inverted microscope (Nikon Instruments) equipped with phase-contrast optics (40x objective) on a vibration isolation platform. A two-electrode configuration was used with potential and gain controlled by an Axopatch 200B potentiostat (Molecular Devices). The data were collected using locally written software in LabView (National Instruments). After the placement of a carbon-fiber microelectrode onto a single platelet sedimented on a poly-L-lysine-coated coverslip, a 3-s bolus of 10 μ M ionomycin and 2 mM Ca^{2+} in Tyrode's buffer was locally delivered onto the platelet via a glass capillary with a 2–3 μ m diameter opening. In amperometry mode, the electrode was held at +700 mV vs Ag/AgCl to detect only secreted serotonin. Recorded data were first filtered at 5 kHz by a built-in four-pole Bessel filter and collected at 20 kHz, allowing submillisecond resolution. In cyclic voltammetry mode, the applied voltage was ramped from –0.4 to 1 V and back to –0.4 at 2000 V s^{-1} once every 2 ms.

Data Processing and Statistical Analysis. The amperometric data were exported, digitally filtered at 1000 Hz, and then analyzed using commercially available software (Minianalysis, Snyptosoft Inc.). The threshold for spike detection was set to 5 times the root-mean-square of the background current collected at the beginning of a given trace. Spike analysis included the determination of the following parameters: I_{amp} , amplitude of spike; T_{rise} , the time from 10% to 90% of the spike amplitude on the rising phase of the spike; T_{decay} , the time from 100% to 1% of the spike amplitude on the decaying phase of the spike; $T_{1/2}$, spike width at the half-maximum; and Q , the spike area. Mean spike characteristics were calculated for each platelet, and then data from platelets exposed to identical experimental conditions were subsequently pooled together for statistical comparison to other platelet populations (45). In addition, foot analyses were performed on the basis of the empirical criteria used within the Minianalysis program. Briefly, the characteristics of a foot feature were determined on the basis of the identification of the inflection point on the rising phase of an amperometric spike. The inflection point, along with the onset of a foot feature and the local baseline for the given amperometric spike, were manually chosen within the analysis software. Then, the foot analysis was performed including the determination of the following parameters: I_{foot} , foot current amplitude at the inflection point; T_{foot} , foot duration from the onset of a foot to the inflection point; and Q_{foot} , foot area, integrating the current over the foot duration. Foot characteristics from individual spikes are pooled rather than their averages obtained from each platelet due to the small number of spikes with a foot feature per amperometry trace. No outliers were excluded and all data are reported as mean \pm standard error of the mean (mean \pm SEM) and subject to two-tailed unpaired Student's t tests.

Acknowledgment: We gratefully thank D. Freeman for her assistance with rabbit blood draws, Dr. A. Harned for the use of a GC-FID instrument, and M. Krumwiede for her help with sample preparation for TEM study. This work is supported by the Kinship Foundation Searle Scholar Program and National Institutes of Health New Innovator Award to Dr. C. Haynes as well as a University of Minnesota Doctoral Dissertation Fellowship to S.G.

Supporting Information Available: This material is available free of charge via the Internet at <http://pubs.acs.org>.

REFERENCES

1. Burgoyne, R. D., and Morgan, A. (2003) Secretory Granule Exocytosis, *Physiol. Rev.* 83, 581–632.
2. Almers, W. (1990) Exocytosis, *Annu. Rev. Physiol.* 52, 607–624.
3. Jahn, R., and Sudhof, T. C. (1999) Membrane Fusion and Exocytosis, *Annu. Rev. Biochem.* 68, 863–911.
4. McNew, J. A. (2008) Regulation of SNARE-Mediated Membrane Fusion during Exocytosis, *Chem. Rev.* 108, 1669–1686.
5. Rizo, J., and Rosenmund, C. (2008) Synaptic Vesicle Fusion, *Nat. Struct. Mol. Biol.* 15, 665–674.
6. Ungar, D., and Hughson, F. M. (2003) SNARE Protein Structure and Function, *Annu. Rev. Cell Dev. Biol.* 19, 493–517.
7. Weber, T., Zemelman, B. V., McNew, J. A., Westermann, B., Gmachl, M., Parlati, F., Sollner, T. H., and Rothman, J. E. (1998) SNAREpins: Minimal Machinery for Membrane Fusion, *Cell* 92, 759–772.
8. Perin, M. S., Fried, V. A., Mignery, G. A., Jahn, R., and Sudhof, T. C. (1990) Phospholipid Binding by a Synaptic Vesicle Protein Homologous to the Regulatory Region of Protein Kinase C, *Nature* 345, 260–263.
9. Churchward, M. A., and Coorsen, J. R. (2009) Cholesterol, Regulated Exocytosis and the Physiological Fusion Machine, *Biochem. J.* 423, 1–14.
10. Wang, N., Kwan, C., Gong, X., de Chaves, E. P., Tse, A., and Tse, F. W. (2010) Influence of Cholesterol on Catecholamine Release from the Fusion Pore of Large Dense Core Chromaffin Granules, *J. Neurosci.* 30, 3904–3911.
11. Zhang, J., Xue, R., Ong, W. Y., and Chen, P. (2009) Roles of Cholesterol in Vesicle Fusion and Motion, *Biophys. J.* 97, 1371–1380.
12. Lang, T., Bruns, D., Wenzel, D., Riedel, D., Holroyd, P., Thiele, C., and Jahn, R. (2001) SNAREs Are Concentrated in Cholesterol-Dependent Clusters that Define Docking and Fusion Sites for Exocytosis, *EMBO J.* 20, 2202–2213.
13. Amatore, C., Arbault, S., Bonifas, I., Bouret, Y., Erard, M., and Guille, M. (2003) Dynamics of Full Fusion during Vesicular Exocytotic Events: Release of Adrenaline by Chromaffin Cells, *ChemPhysChem.* 4, 147–154.
14. Travis, E. R., and Wightman, R. M. (1998) Spatio-Temporal Resolution of Exocytosis from Individual Cells, *Annu. Rev. Biophys. Biomol. Struct.* 27, 77–103.
15. Uchiyama, Y., Maxson, M. M., Sawada, T., Nakano, A., and Ewing, A. G. (2007) Phospholipid Mediated Plasticity in Exocytosis Observed in PC12 Cells, *Brain Res.* 1151, 46–54.
16. Amatore, C., Arbault, S., Bouret, Y., Guille, M., Lemaitre, F., and Verchier, Y. (2006) Regulation of Exocytosis in Chromaffin Cells by Trans-Insertion of Lysophosphatidylcholine and Arachidonic Acid into the Outer Leaflet of the Cell Membrane, *ChemBioChem.* 7, 1998–2003.

17. Reed, G. L., Fitzgerald, M. L., and Polgar, J. (2000) Molecular Mechanisms of Platelet Exocytosis: Insights into the "Secrete" Life of Thrombocytes, *Blood*, **96**, 3334–3342.
18. Holmsen, H., and Weiss, H. J. (1979) Secretory Storage Pools in Platelets, *Annu. Rev. Med.* **30**, 119–134.
19. Amatore, C., Bouret, Y., Travis, E. R., and Wightman, R. M. (2000) Interplay between Membrane Dynamics, Diffusion and Swelling Pressure Governs Individual Vesicular Exocytotic Events during Release of Adrenaline by Chromaffin Cells, *Biochimie* **82**, 481–496.
20. Amatore, C., Arbault, S., Guille, M., and Lemaître, F. (2008) Electrochemical Monitoring of Single Cell Secretion: Vesicular Exocytosis and Oxidative Stress, *Chem. Rev.* **108**, 2585–2621.
21. Tabares, L., Lindau, M., and Alvarez de Toledo, G. (2003) Relationship between Fusion Pore Opening and Release during Mast Cell Exocytosis Studied with Patch Amperometry, *Biochem. Soc. Trans.* **31**, 837–841.
22. Ge, S., Wittenberg, N. J., and Haynes, C. L. (2008) Quantitative and Real-Time Detection of Secretion of Chemical Messengers from Individual Platelets, *Biochemistry* **47**, 7020–7024.
23. Ge, S., White, J. G., and Haynes, C. L. (2009) Quantal Release of Serotonin from Platelets, *Anal. Chem.* **81**, 2935–2943.
24. Smith, C. B., and Betz, W. J. (1996) Simultaneous Independent Measurement of Endocytosis and Exocytosis, *Nature* **380**, 531–534.
25. McNicol, A., and Israels, S. J. (1999) Platelet Dense Granules: Structure, Function and Implications for Haemostasis, *Thromb. Res.* **95**, 1–18.
26. Ungar, A., and Phillips, J. H. (1983) Regulation of the Adrenal Medulla, *Physiol. Rev.* **63**, 787–843.
27. Schubert, P., Devine, D. V. (2010) *De Novo* Protein Synthesis in Mature Platelets: A Consideration for Transfusion Medicine. *Vox Sang.* Published online March 21, 2010, DOI: 10.1111/j.1423-0410.2010.01333.x.
28. Christian, A. E., Haynes, M. P., Phillips, M. C., and Rothblat, G. H. (1997) Use of Cyclodextrins for Manipulating Cellular Cholesterol Content, *J. Lipid Res.* **38**, 2264–2272.
29. Zidovetzki, R., and Levitan, I. (2007) Use of Cyclodextrins to Manipulate Plasma Membrane Cholesterol Content: Evidence, Misconceptions and Control Strategies, *Biochim. Biophys. Acta* **1768**, 1311–1324.
30. Lange, Y., Swaisgood, M. H., Ramos, B. V., and Steck, T. L. (1989) Plasma Membranes Contain Half the Phospholipid and 90% of the Cholesterol and Sphingomyelin in Cultured Human Fibroblasts, *J. Biol. Chem.* **264**, 3786–3793.
31. Chow, R. H., von Ruden, L., and Neher, E. (1992) Delay in Vesicle Fusion Revealed by Electrochemical Monitoring of Single Secretory Events in Adrenal Chromaffin Cells, *Nature* **356**, 60–63.
32. Murray, D. H., and Tamm, L. K. (2009) Clustering of Syntaxin-1A in Model Membranes is Modulated by Phosphatidylinositol 4,5-Bisphosphate and Cholesterol, *Biochemistry* **48**, 4617–4625.
33. Predescu, S. A., Predescu, D. N., Shimizu, K., Klein, I. K., and Malik, A. B. (2005) Cholesterol-Dependent Syntaxin-4 and SNAP-23 Clustering Regulates Caveolar Fusion with the Endothelial Plasma Membrane, *J. Biol. Chem.* **280**, 37130–37138.
34. Ohara-Imaizumi, M., Nishiwaki, C., Kikuta, T., Kumakura, K., Nakamichi, Y., and Nagamatsu, S. (2004) Site of Docking and Fusion of Insulin Secretory Granules in Live MIN6 Beta Cells Analyzed by TAT-Conjugated Anti-Syntaxin 1 Antibody and Total Internal Reflection Fluorescence Microscopy, *J. Biol. Chem.* **279**, 8403–8408.
35. Chen, D., Bernstein, A. M., Lemons, P. P., and Whiteheart, S. W. (2000) Molecular Mechanisms of Platelet Exocytosis: Role of SNAP-23 and Syntaxin 2 in Dense Core Granule Release, *Blood*, **95**, 921–929.
36. Dufourc, E. J. (2008) Sterols and Membrane Dynamics, *J. Chem. Biol.* **1**, 63–77.
37. Gimpl, G., Wiegand, V., Burger, K., and Fahrenholz, F. (2002) Cholesterol and Steroid Hormones: Modulators of Oxytocin Receptor Function, *Prog. Brain Res.* **139**, 43–55.
38. Xu, X., and London, E. (2000) The Effect of Sterol Structure on Membrane Lipid Domains Reveals how Cholesterol can Induce Lipid Domain Formation, *Biochemistry* **39**, 843–849.
39. Markin, V. S., and Albanesi, J. P. (2002) Membrane Fusion: Stalk Model Revisited, *Biophys. J.* **82**, 693–712.
40. Kozlovsky, Y., and Kozlov, M. M. (2002) Stalk Model of Membrane Fusion: Solution of Energy Crisis, *Biophys. J.* **82**, 882–895.
41. Chen, Z., and Rand, R. P. (1997) The Influence of Cholesterol on Phospholipid Membrane Curvature and Bending Elasticity, *Biophys. J.* **73**, 267–276.
42. Jackson, M. B., and Chapman, E. R. (2008) The Fusion Pores of Ca^{2+} -Triggered Exocytosis, *Nat. Struct. Mol. Biol.* **15**, 684–689.
43. Churchward, M. A., Rogasevskaia, T., Brandman, D. M., Khosravani, H., Nava, P., Atkinson, J. K., and Coorsen, J. R. (2008) Specific Lipids Supply Critical Negative Spontaneous Curvature—an Essential Component of Native Ca^{2+} -Triggered Membrane Fusion, *Biophys. J.* **94**, 3976–3986.
44. Taraska, J. W., and Almers, W. (2004) Bilayers Merge Even when Exocytosis Is Transient, *Proc. Natl. Acad. Sci. U.S.A.* **101**, 8780–8785.
45. Colliver, T. L., Hess, E. J., Pothos, E. N., Sulzer, D., and Ewing, A. G. (2000) Quantitative and Statistical Analysis of the Shape of Amperometric Spikes Recorded from Two Populations of Cells, *J. Neurochem.* **74**, 1086–1097.